Article:

Mobasher, N., Bernal, S.A., Hussain, O.H. et al. (3 more authors) (2014) Characterisation of Ba(OH)(2)-Na2SO4-blast furnace slag cement-like composites for the immobilisation of sulfate bearing nuclear wastes. Cement and Concrete Research, 66. pp. 64-74. ISSN 0008-8846

https://doi.org/10.1016/j.cemconres.2014.07.006

Postprint of a paper published in *Cement and Concrete Research*, 66(2014):64-74. Version of record is available at http://dx.doi.org/10.1016/j.cemconres.2014.07.006

Characterisation of $Ba(OH)_2$–Na_2SO_4-blast furnace slag cement-like composites for the immobilisation of sulphate bearing nuclear wastes

Neda Mobasher[1], Susan A. Bernal[1], Oday H. Hussain[1], David C. Apperley[2], Hajime Kinoshita[1], John L. Provis[1*]

[1] *Immobilisation Science Laboratory, Department of Materials Science & Engineering, The University of Sheffield, Sheffield S1 3JD, United Kingdom*

[2] *Solid-State NMR Group, Department of Chemistry, Durham University, Durham DH1 3LE, United Kingdom*

* To whom correspondence should be addressed. Email j.provis@sheffield.ac.uk, phone +44 114 222 5490, fax +44 114 222 5493

Abstract

Soluble sulphate ions in nuclear waste can have detrimental effects on cementitious wasteforms and disposal facilities based on Portland cement. As an alternative, $Ba(OH)_2$-Na_2SO_4-blast furnace slag composites are studied for immobilisation of sulphate-bearing nuclear wastes. Calcium aluminosilicate hydrate (C-A-S-H) with some barium substitution is the main binder phase, with barium also present in the low solubility salts $BaSO_4$ and $BaCO_3$, along with Ba-substituted calcium sulphoaluminate hydrates, and a hydrotalcite-type layered double hydroxide. This reaction product assemblage indicates that $Ba(OH)_2$ and Na_2SO_4 act as alkaline activators and control the reaction of the slag in addition to forming insoluble $BaSO_4$, and this restricts sulphate availability for further reaction as long as sufficient $Ba(OH)_2$ is added. An increased content of $Ba(OH)_2$ promotes a higher degree of reaction, and the formation of a highly cross-linked C-A-S-H gel. These $Ba(OH)_2$-Na_2SO_4-blast furnace slag composite binders could be effective in the immobilisation of sulphate-bearing nuclear wastes.

Keywords: alkali-activated cements; granulated blast furnace slag; sulphate-bearing nuclear waste; barium; microstructure

1. Introduction

The immobilisation of sulphate bearing radioactive waste generated in the nuclear industry is difficult to achieve effectively via vitrification or traditional cementing processes, which are the most common methodologies used worldwide for the immobilisation of low and intermediate level nuclear wastes. The presence of soluble sulphate during vitrification causes phase separation in borosilicate glass [1], and in the case of cement-based materials it can promote microstructural changes in the long term [2-4], such as expansion and cracking through the process of internal sulphate attack, which may result in the release of radionuclides into the environment. If sulphate-containing nuclear waste is not treated and encapsulated effectively, it can also interact with any Portland cement-based backfill or structural concrete used in a repository, potentially causing decay of the repository structure through sulphate attack processes. Calcium aluminate or sulphoaluminate cement-based materials can sometimes accommodate much higher sulphate contents without undergoing degradation processes, but also offer handling and processing challenges in this application.

Asano et al. [5] proposed an alternative method for the solidification/stabilisation of sulphate-rich aqueous low level wastes using $Ba(OH)_2$ and slag, via a two-step process in which a cement-like solid can be formed. In their method, Na_2SO_4 (simulated waste) solution was mixed with $Ba(OH)_2$ in the first step, stabilising the sulphate ions through the precipitation of the highly insoluble phase $BaSO_4$ and releasing NaOH (reaction 1), followed by a second step of blending the alkaline $BaSO_4$-containing slurry (produced in the first step) with blast furnace slag (BFS) to produce a cement-like solid (reaction 2).

$$Ba(OH)_2 + Na_2SO_4 \rightarrow BaSO_4 + 2NaOH \qquad (1)$$

$$NaOH + \text{BFS (+ any remaining/excess } Ba(OH)_2 \text{ or } Na_2SO_4) \rightarrow \text{solid binder} \qquad (2)$$

Recently, Mobasher et al. [6] published a proof-of-concept of a one-step process to produce solid wasteforms with comparable chemistry to those assessed by Asano et al. [5] for immobilisation of sulphate bearing aqueous waste, formulating $Ba(OH)_2$-Na_2SO_4-BFS composites. In this one-step process, reactions (1) and (2) take place simultaneously. The reaction scheme developed effectively results in an alkali-activation process, with the $Ba(OH)_2$ and Na_2SO_4, as well as NaOH generated in situ, interacting with the slag to form a hardened binder. A single-step approach has advantages from an operational point of view, compared with that proposed by Asano et al. [5], as less manipulation of the aqueous waste is favourable for adequate disposal. Cement-like systems of this type would be beneficial not only because of the formation of very low-solubility $BaSO_4$ [7], but also because $BaSO_4$ can enhance the radiation shielding properties of a wasteform or concrete due to the high atomic number of Ba [8]. Additionally, the presence of $BaSO_4$ in these binders can be useful for co-precipitation of radionuclides such as ^{90}Sr that can be present in the aqueous waste [9].

When BFS reacts with a source of alkalis to form a hardened binder, the main reaction product and strength-giving phase is a calcium-silicate-hydrate (C-S-H) type phase with a low Ca/Si ratio and a significant degree of aluminium substitution, termed C-A-S-H [10, 11]. The structure and composition of the C-A-S-H and secondary reaction products forming in alkali-activated slag binders are strongly dependent on the nature of the activator selected [12-15], the activation conditions adopted [16], and the chemical composition of the slag used [17-19]. In the case of silicate- and hydroxide-activated slags, for instance, layered double hydroxide compounds have been observed [20-23]. When Na_2SO_4 is used as the sole activator, the main secondary product is ettringite [24, 25], because of the increased content of sulphate available in the system.

It is, therefore, important to understand the activation reaction of the slag in these cementitious wasteforms, as the development of the main binding phase can have a significant influence on the chemistry and microstructure of the system, which in return has a direct impact on radionuclide binding and the permeability of gases and liquids through the solid, and thus wasteform performance. This is of particular interest for the $Ba(OH)_2$-Na_2SO_4-BFS composite system, as this system has different constituents which can potentially act as an activator i.e., $Ba(OH)_2$, Na_2SO_4 and NaOH. The published literature does not contain detailed chemical or microstructural characterisation of $Ba(OH)_2$-activated slags, and therefore the role of $Ba(OH)_2$ in the activation and structural development of these materials is still unknown.

In this study $Ba(OH)_2$-Na_2SO_4-BFS composite pastes, formulated with different $Ba(OH)_2$ to Na_2SO_4 ratios, are evaluated via X-ray diffraction (XRD), nuclear magnetic resonance (NMR), and scanning electron microscopy (SEM) coupled with energy dispersive X-ray (EDX) spectroscopy. To determine the individual roles of $Ba(OH)_2$ and Na_2SO_4 in the alkali-

Postprint of a paper published in *Cement and Concrete Research*, 66(2014):64-74. Version of record is available at http://dx.doi.org/10.1016/j.cemconres.2014.07.006

activation reaction of the slag, samples activated with each compound individually are also evaluated, in addition to samples activated with NaOH to provide comparative information.

2. Experimental programme

2.1.Materials

A blast furnace slag (BFS) from Redcar steelworks with a specific surface of 286 m^2/kg was used as the main solid precursor, and its chemical composition is presented in Table 1. Barium hydroxide octahydrate ($Ba(OH)_2 \cdot 8H_2O$, 97% purity) and sodium sulphate (Na_2SO_4, 99% purity) from Alfa Aesar, and sodium hydroxide (NaOH, general purpose grade) from Fisher Scientific, were used to produce the composites.

Table 1. Composition of blast furnace slag (BFS), from X-ray fluorescence analysis. LOI is loss on ignition at 1000°C

Component as oxides	**CaO**	**SiO_2**	**Al_2O_3**	**Fe_2O_3**	**MgO**	**K_2O**	**Na_2O**	**SO_3**	**others**	**LOI**
Weight %	38.8	35.8	13.4	0.9	7.6	0.4	0.3	0.7	1.2	0.9

2.2.Sample preparation and tests conducted

A simulated aqueous sulphate-bearing waste (10 wt.% Na_2SO_4) was prepared by dissolving solid anhydrous Na_2SO_4 in distilled water at 40°C, and then mixed with a homogeneous blend of unreacted BFS and powdered $Ba(OH)_2 \cdot 8H_2O$ in a sealed plastic container. The samples were manually shaken for 2 to 5 minutes at room temperature, and then mixed for 5 more minutes using a Whirh Mixer. Detailed formulations of the specimens produced are given in Table 2.

Table 2. Formulations of Na_2SO_4-$Ba(OH)_2$-BFS composites and alkali-activated BFS. The water/binder (w/b) ratio column includes water incorporated as part of the hydrated barium hydroxide.

Sample ID	**Ba^{2+}:SO_4^{2-} molar ratio**	**w/b**	**BFS (g)**	**H_2O (g)**	**Na_2SO_4 (g)**	**$Ba(OH)_2{\cdot}8H_2O$ (g)**	**NaOH (g)**
BFS + Na_2SO_4		0.34	100	34	39	0	0
BFS + $Ba(OH)_2$		0.37	100	37	0	11.23	0
BFS + NaOH		0.34	100	34	0	0	2.2
M1.0	1.0 : 1.0	0.36	100	36	39	8.64	0
M1.3	1.3 : 1.0	0.37	100	37	39	11.23	0

The same procedure was used to prepare the reference samples for the assessment of the role of $Ba(OH)_2$, Na_2SO_4 and NaOH in the activation procedure. The contents of $Ba(OH)_2$ and Na_2SO_4 in the reference specimens were based on the formulation of M1.3, but using each of the activator components individually. The amount of NaOH used in that reference sample was calculated to match the quantity which would be generated by a stoichiometric chemical reaction between the amounts of Na_2SO_4 and $Ba(OH)_2$ present in sample M1.3 to produce $BaSO_4$ and NaOH.

Specimens were cured for 180 days at room temperature under sealed conditions, then demoulded, crushed and immersed in acetone to arrest the reaction process. After several days, the samples were removed from the acetone, dried to remove the solvent, and desiccated under vacuum. The dried samples were kept in sealed containers prior to analysis to avoid carbonation.

Characterisation of the pastes was conducted by:

- X-ray diffraction (XRD), using a Siemens D5000 X-ray diffractometer with monochromatic Cu Kα radiation, operated at a step size of 0.02° and a scanning speed of 0.5°/min between 5° and 55° 2θ. Specimens were ground using an agate mortar and pestle, and sieved to < 63μm prior to the measurement.
- Thermogravimetric analysis (TGA), using a Perkin Elmer Pyris 1 TGA. Approximately 40 mg of sample was placed in an alumina crucible. The samples were heated under a flowing nitrogen atmosphere at a heating rate of 10°C/min from room temperature up to 1000°C.

- Solid-state ^{29}Si MAS NMR spectra were collected at 59.56 MHz on a Varian Unity Inova 300 (7.05 T) spectrometer using a probe for 7.5 mm o.d. zirconia rotors and a spinning speed of 5 kHz. The ^{29}Si MAS experiments employed a 90° pulse of duration 5 µs, a relaxation delay of 5 s and 14000 scans. Solid-state ^{27}Al MAS NMR spectra were acquired at 104.198 MHz, using a Varian VNMRS 400 (9.4T) spectrometer and a probe for 4 mm o.d. zirconia rotors and a spinning speed of 14 kHz with a pulse width of 1 µs (approximately 25°), a relaxation delay of 0.2 s, and a minimum of 7000 scans. ^{23}Na MAS NMR spectra were collected on the VNMRS spectrometer at 105.78 MHz using a probe for 4 mm o.d. zirconia rotors and a spinning speed of 10 kHz with a pulse width of 1 µs (approximately 25°), a relaxation delay of 1 s, and a minimum of 2000 scans. ^{29}Si, ^{27}Al, ^{23}Na chemical shifts are referenced to external samples of tetramethylsilane (TMS), a 1.0 M aqueous solution of $Al(NO_3)_3$, and a 0.1M aqueous solution of NaCl, respectively.
- Scanning electron microscopy (SEM), using a JEOL electron microscope, JSM 6400, with a backscattered electron detector and an accelerating voltage of 20 keV. Epoxy resin (EpoxiCure ^{TM}) was poured over the samples, which were then held under vacuum to minimise entrapped air. The samples were removed from the vacuum after approximately 15 minutes and left for 24 hours to harden before sanding manually with grinding papers of 400 and 1200 grit SiC. Samples were then polished with 1 µm and 0.25 µm diamond pastes and polishing cloths. The samples were finally coated with carbon using an Edwards ‘speedivac’ carbon coating unit and silver dagged to make them electrically conductive before analysis.

3. Results and discussion

3.1. X-ray diffraction

The X-ray diffractograms of the reference samples of BFS activated with Na_2SO_4, NaOH and $Ba(OH)_2$ are compared with that of the unreacted slag in Figure 1. The unreacted slag is predominantly amorphous, and contains minor traces of the melilite type phase åkermanite ($Ca_2MgSi_2O_7$, powder diffraction file, PDF, #076-0841), and calcite ($CaCO_3$, PDF #005-0586) due to slight weathering. Upon activation with Na_2SO_4, formation of ettringite (PDF # 041-1451) is identified, in agreement with what has previously been reported for similar systems [24, 25]. A small peak at 11.3° 2θ is also observed in these samples, and is assigned to a layered double hydroxide in the hydrotalcite group ($Mg_6Al_2(CO_3)(OH)_{16}\cdot 4H_2O$, PDF # 089-0460). In alkali-activated slags with moderate to high MgO contents, such layered double hydroxides are usually produced as a secondary reaction product [17, 19]. Disordered C-S-H type gel products are also identified in all samples by a very broad peak centred just below 30° 2θ.

In the NaOH-activated slag, ettringite is not forming, consistent with the absence of sulphates in the system, and instead hemicarbonate-AFm ($(CaO)_3\cdot Al_2O_3\cdot 0.5CaCO_3\cdot 12H_2O$, PDF # 036-0129) is observed along with hydrotalcite. Identification of AFm type phases in NaOH-activated slag binders is difficult to achieve via X-ray diffraction [20, 22, 26]; however, formation of this type of phase has been suggested through analysis of NaOH-activated slag binders by NMR spectroscopy [23, 27], potentially as a crystallographically disordered phase intermixed with the C-A-S-H products [28].

In the $Ba(OH)_2$ activated slag sample, a reflection consistent with the position of the main hydrotalcite peak just above 10° 2θ was observed, with a slight shift towards lower 2θ compared to the hydrotalcite reference pattern. This indicates an increased *d*-spacing in this phase, which may correspond to some Ba^{2+} incorporation as a larger cation substituting for the smaller Mg^{2+}. Although this has not previously been noted as a possibility in the literature for such phases, and the cationic radii are very different, Glasser [29] has reported substitution of Ca^{2+} by Ba^{2+} in crystalline cement phases. In addition, it has been observed that AFm phases, a type of layered double hydroxides are highly susceptible to cation exchange at room temperature, with compositions very sensitive to their local chemical environment [30]., Therefore, Ba substitution in layered double hydroxides such as hydrotalcite-like and AFm type phases could be plausible in the $Ba(OH)_2$-activated slag binder.

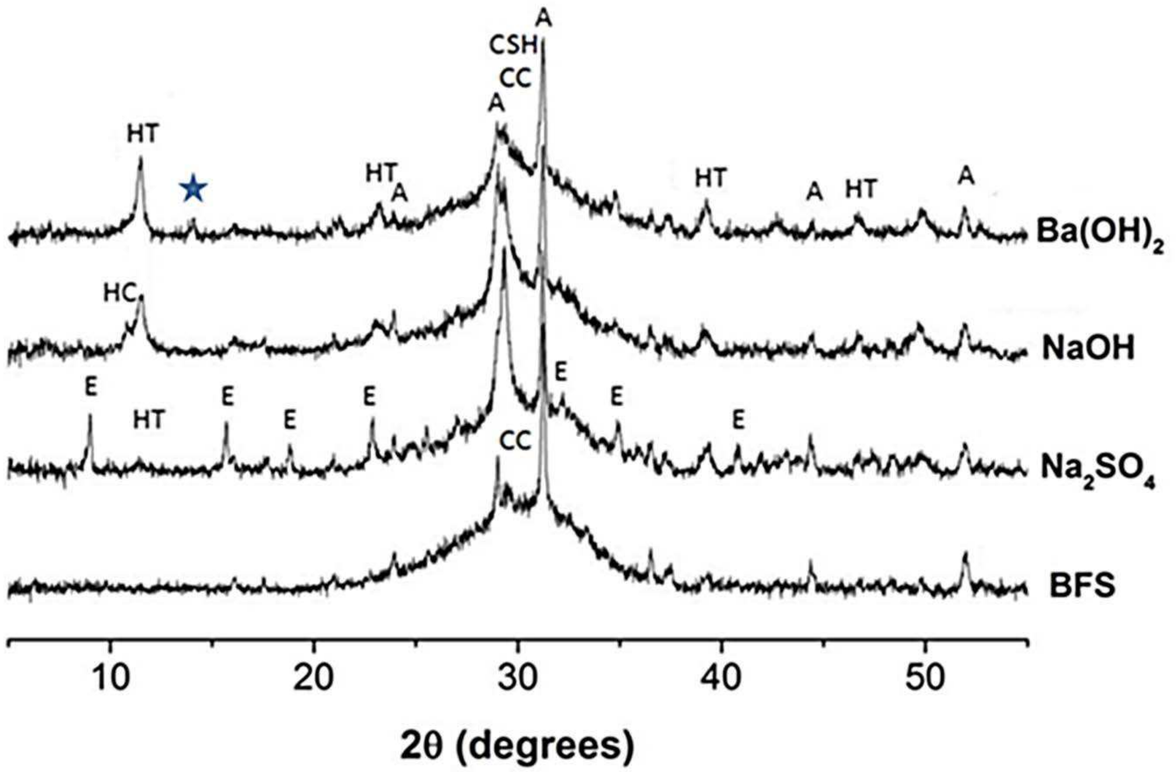

Figure 1. X-ray diffractograms of unreacted BFS, Na_2SO_4-activated BFS, NaOH-activated BFS and $Ba(OH)_2$-activated BFS pastes. Peaks marked are åkermanite (A), calcite (CC), ettringite (E), hemicarbonate (HC), hydrotalcite (HT) and C-A-S-H (CSH). The peak marked with★ matches one of the stronger reflections of dresserite ($BaAl_2(CO_3)_2(OH)_4 \cdot H_2O$); however, the main dresserite reflection (8.09° 2θ) is not observed, and so the identification of this phase is considered tentative.

In the composite binders M1.0 and M1.3 (Figure 2), åkermanite and calcite from the unreacted slag are again identified, along with formation of barite ($BaSO_4$, PDF #24-1035) and witherite ($BaCO_3$, PDF #45-1471). This indicates that barium is reacting with the excess sulphate and carbonates present in the system to form stable insoluble Ba-rich compounds. The intensities of the peaks assigned to $BaSO_4$ appear to increase with higher contents of $Ba(OH)_2$, suggesting that the addition of $Ba(OH)_2$ promotes a higher extent of $BaSO_4$ formation. A layered double hydroxide with a hydrotalcite type structure is also formed as a secondary reaction product in these systems, indicating that the formation of $BaSO_4$ is not hindering the development of secondary phases in the alkali-activated composite.

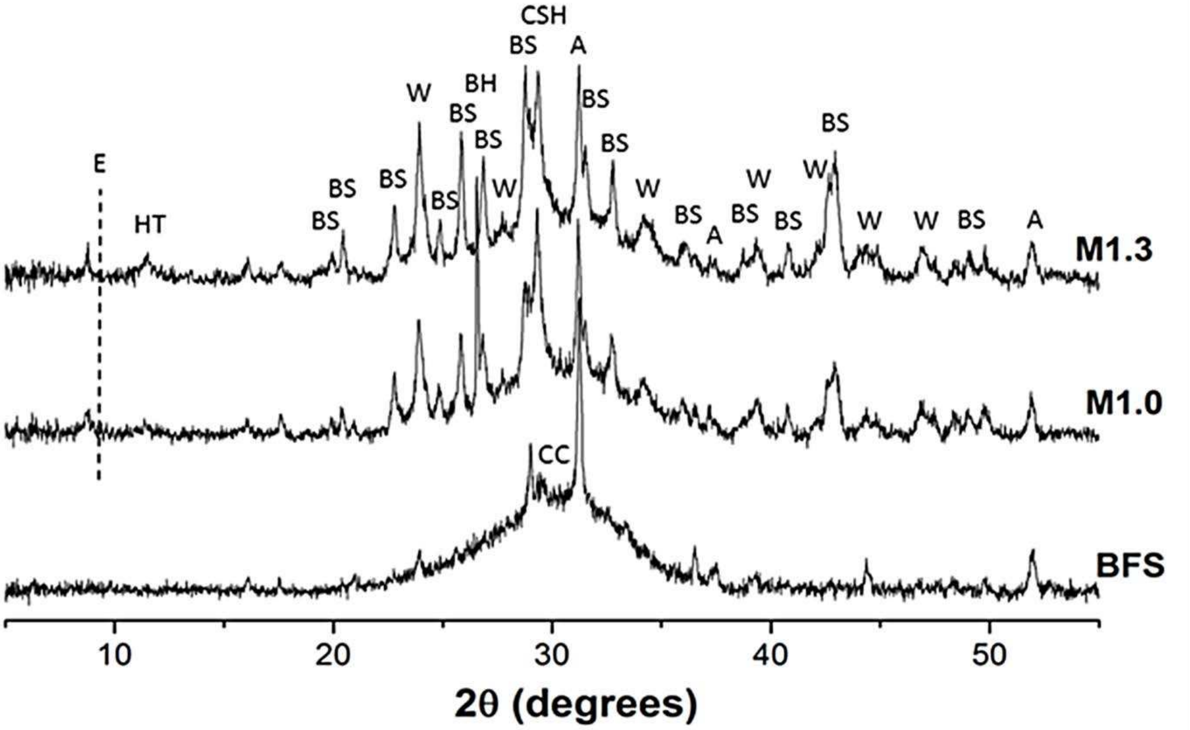

Figure 2. X-ray diffractograms of unreacted slag and Na_2SO_4-$Ba(OH)_2$-BFS composites as a function of the Ba^{2+} to SO_4^{2-} molar ratio. Peaks marked are $BaSO_4$ (BS), åkermanite (A), calcite (CC), witherite (W), ettringite (E), hydrotalcite (HT) and C-A-S-H (CSH). The dashed line indicates the position of the main (100) peak of ettringite.

In these composites, independent of the $Ba(OH)_2$ content, the formation of a compound with a peak at 8.50° 2θ is observed (Figure 2). As the peak position is slightly shifted to lower 2θ when compared with the main reflection peak of ettringite (9.0° 2θ), it is likely that in presence of $Ba(OH)_2$, formation of a Ba-containing AFt type phase takes place. The substitution of Ba^{2+} in the Ca^{2+} sites in ettringite structure has previously been reported [29, 31], and Ba-bearing ettringite has a larger *d*-spacing than pure ettringite [32], shifting the peak to lower angle as observed in these samples. Utton et al. [33] identified, in a 1:9 Portland cement/BFS system containing $BaCO_3$, that the formation of ettringite and precipitation of $BaSO_4$ occur simultaneously, competing for the sulphate ions in the solution. After extended times of curing in those systems, ettringite decomposed to form calcium monocarboaluminate (AFm), calcite and $BaSO_4$, by reacting with the free Ba^{2+} ions. Considering that the compounds identified as being stable by Utton et al. [33] are similar to those which form in the $Ba(OH)_2$-Na_2SO_4-slag composites here, significant changes in the phase assemblage of the composites are unlikely to occur at advanced times of curing.

The results obtained here reveal that in the composites assessed in this study, as formation of ettringite takes place as a consequence of the Na_2SO_4-activation of slag, not all of the sulphate is directly consumed according to equation (1) by $BaSO_4$ precipitation. Na_2SO_4 will continue promoting the formation of ettringite in the system when its amount exceeds the capacity of $Ba(OH)_2$ to immediately form $BaSO_4$. This observation differs from the trends identified in studies evaluating the effects of $Ba(OH)_2$ or $BaCO_3$ on the structures of synthetic ettringite and thaumasite [34-36], where the formation of ettringite was supressed or ettringite is completely decomposed. In these studies, a large quantity of $Ba(OH)_2$ was used, suggesting that the content of $Ba(OH)_2$ would need to be increased in the composite systems to hinder the formation of ettringite.

3.2 Thermogravimetry

Figure 3 shows the differential thermograms (DTG) of Na_2SO_4-activated BFS, NaOH-activated BFS and $Ba(OH)_2$-activated BFS pastes. The total loss of weight up to 1000°C for Na_2SO_4-activated BFS is 13.9%, for NaOH-activated BFS 12.06%, and for $Ba(OH)_2$-activated BFS 16.4%.

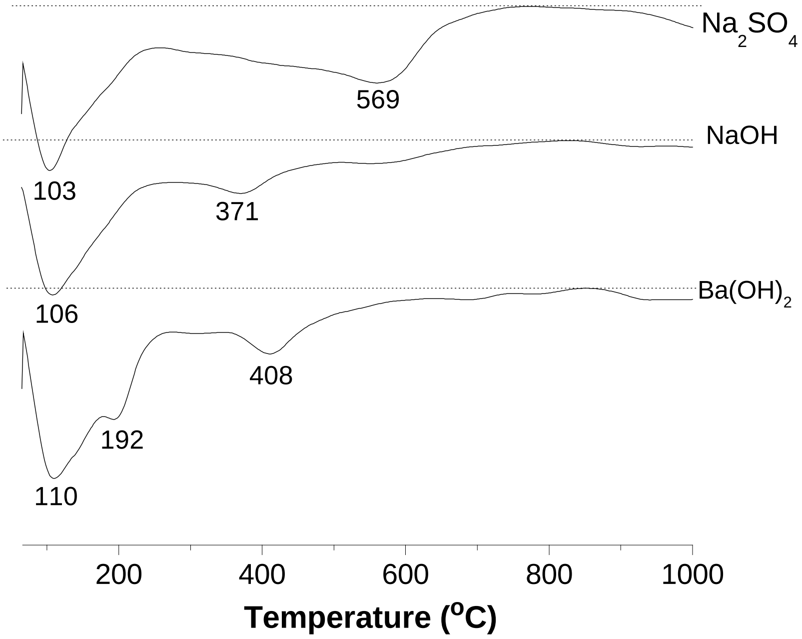

Figure 3. Differential thermograms (mass loss downwards) of alkali-activated BFS with different alkaline activators. Dashed lines show the baseline for each data set.

In the Na_2SO_4-activated BFS, a high intensity peak between 70°C and 200°C is observed, which is attributed to the release of evaporable water in the system, and the start of the dehydration of ettringite [37], as was identified through XRD (Figure 1). The progressive weight loss between 200°C and 400°C is assigned to the decomposition of the C-A-S-H [38] also identified through XRD. The low intensity shoulder around 569°C is attributed to the decomposition of calcite [39]. In NaOH-activated and $Ba(OH)_2$-activated samples, the weight loss around 200ºC and 400ºC is assigned to the hydrotalcite like-phase and the decomposition of AFm type compounds present in the sample [40, 41]. The first weight loss peak around 192ºC in the $Ba(OH)_2$-activated sample corresponds to the removal of the interlayer water molecules of hydrotalcite, and the second peak around 408ºC is assigned to the dehydroxylation of the brucite-like layers [42]. The hydrotalcite peaks are more distinct in the BFS+$Ba(OH)_2$ sample, consistent with a higher extent of reaction of the slag, and potentially more ordering of the structure of this phase when using $Ba(OH)_2$ as the alkaline activator.

Figure 4 shows the differential thermograms (DTG) of unreacted slag and Na_2SO_4-$Ba(OH)_2$-BFS composites with different Ba^{2+}:SO_4^{2-} molar ratios. The total weight loss up to 1000°C for M1.0 is 14.58%, and 10.25% for M1.3. The $BaSO_4$ decomposition temperature is above 1000°C [36], and therefore it is not observed in these thermogravimetry data.

In M1.0 a higher intensity weight loss is observed below 270°C compared with M1.3, which suggests a larger amount of evaporable water in that sample, or potentially the formation of a larger amount of hydration products with water less tightly bonded to the structure than in M1.3. Even though AFm phases were not identified via X-ray diffraction in these samples (Figure 2), it is possible that the minor contributions observed at 144°C and 291°C are associated with decomposition of partially ordered calcium monosulphoaluminate hydrates [41]. Weight losses at 568ºC and ~740°C are assigned to the decomposition of the calcium carbonate products present in the composite samples [43]. Decomposition of the hydrotalcite type phase observed in these composites is detected at 185°C and 394°C, and the minor weight loss above 800°C is assigned to decomposition of witherite [36].

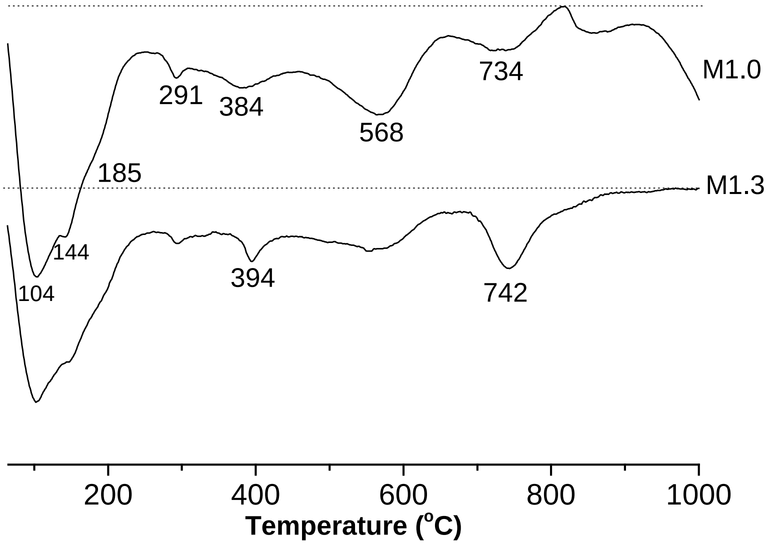

Figure 4. Differential thermograms (mass loss downwards) for Na_2SO_4-$Ba(OH)_2$-BFS composites with different Ba^{2+}:SO_4^{2-} molar ratios. Dashed lines show the baseline for each data set

3.3 Solid-state ^{29}Si MAS NMR spectroscopy

Solid state ^{29}Si MAS NMR can provide information regarding the fractions of silicon present in various tetrahedral environments in silicates [44]. Deconvolutions of the spectra collected here were carried out according to the procedure described in [43]. An example of a deconvoluted spectrum is shown in Figure 5.

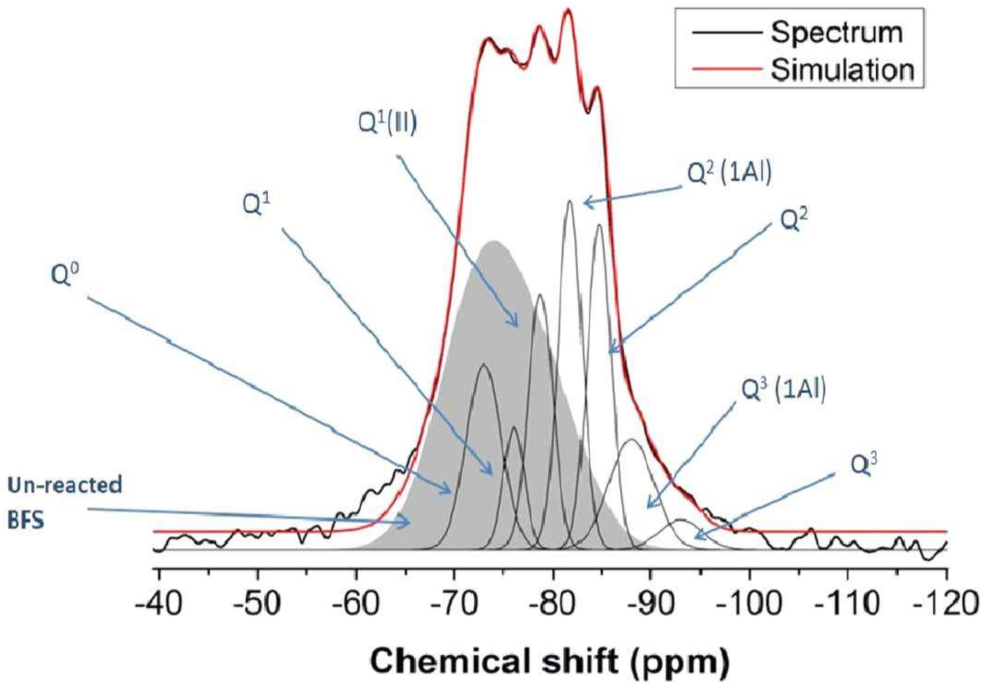

Figure 5. Deconvoluted ^{29}Si MAS NMR spectrum of composite M1.0. The grey area corresponds to the fraction of unreacted slag.

The resonances identified in the deconvoluted spectra are assigned to connectivity states based on the information available for cements [28, 45], alkali-activated slags [19, 43] and aluminosilicate zeolite systems [44]. It has been proposed that it is possible to determine the degree of reaction of alkali-activated slag binders through the deconvolution of ^{29}Si MAS NMR spectra, as the spectral line shape of the remnant unreacted slag in the activated samples is similar to the line shape of the anhydrous slag [46], and a similar approach was adopted in this study. The lineshape in the downfield region (-60 to -70 ppm) in all reaction product spectra is consistent with this hypothesis of congruent or near-congruent dissolution of the slag, as there is not a notable change in the profile in this region between the spectra of the anhydrous slag and the composite cements.

Figure 6A shows the ^{29}Si MAS NMR spectra of Na_2SO_4-activated BFS, NaOH-activated BFS and $Ba(OH)_2$-activated BFS pastes, while Figure 6B shows those of the unreacted slag, and the M1.0 and M1.3 composites. The unreacted slag has a line shape comparable to the spectrum reported for åkermanite [43], which is identified as the main crystalline phase in the slag used in this study (Figure 2) with a resonance centred at -74 ppm. A reduction of this peak indicates the reaction of the slag in the hydrated samples. In the activated samples resonances between -80 ppm and -90 ppm are identified, consistent with the formation of a C-A-S-H type phase. In particular, resonances between -82 ppm and -85 ppm, corresponding to Q^2(1Al) and Q^2 sites respectively, are assigned to this Al-substituted C-S-H type gel with a tobermorite type structure [28, 47].

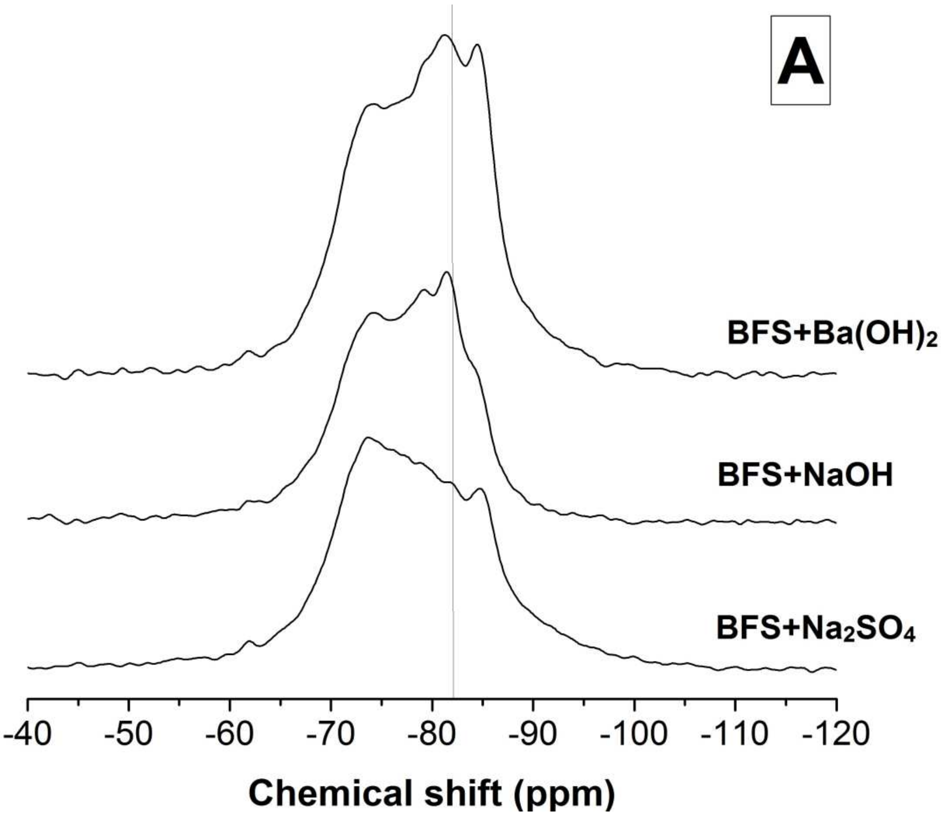

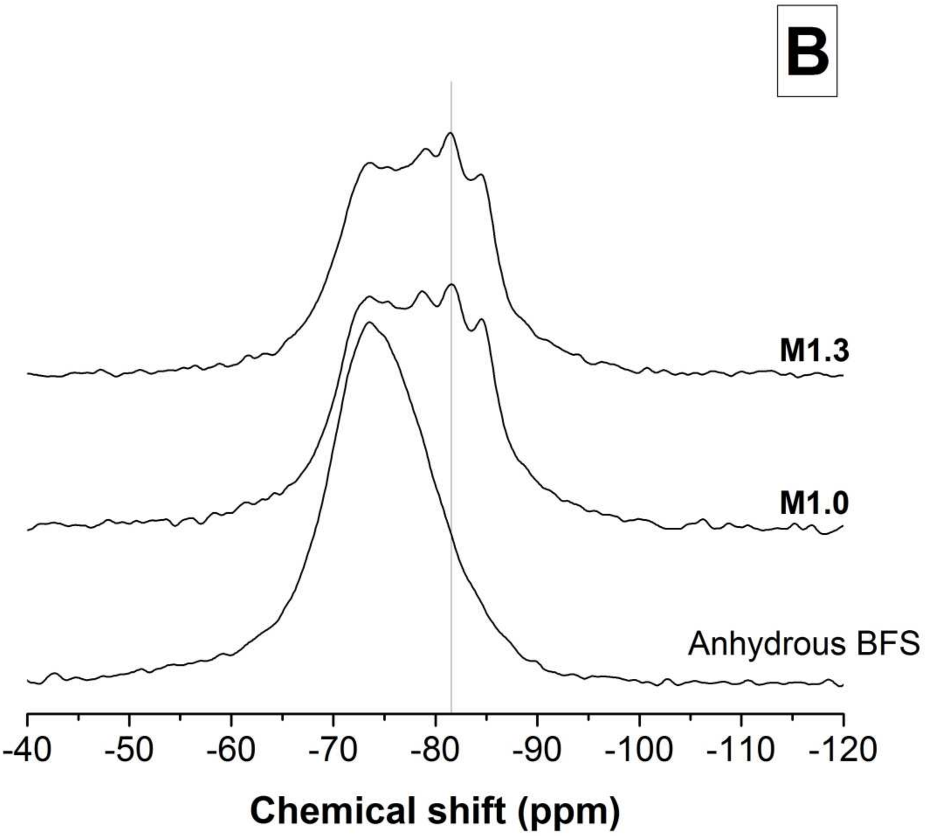

Figure 6. ^{29}Si MAS NMR spectra of **(A)** Na_2SO_4-activated BFS, NaOH-activated BFS and $Ba(OH)_2$-activated BFS pastes, and **(B)** unreacted slag, and Na_2SO_4-$Ba(OH)_2$-BFS composites M1.0 and M1.3. Dashed lines indicate the position of Q^2(1Al) sites.

Figure 6A shows the reduction of the Q^2(1Al) site (-82 ppm) in the spectrum of the Na_2SO_4-activated sample compared to the other activated samples, indicating a reduced degree of Al incorporation in the C-A-S-H product. This could be associated with the fact that most of the Al available in the system is consumed in the formation of ettringite in this formulation (Figure 1).

In the spectra of the composites M1.0 and M1.3 shown in Figure 6B, the intensity of the broad unreacted slag feature centred at -74 ppm decreases with the increased addition of $Ba(OH)_2$, showing a higher extent of reaction, as shown in Table 3. The addition of $Ba(OH)_2$ in the composite samples seems to favour the incorporation of Al in the C-A-S-H type gel, associated with the increasing intensity of the Q^2(1Al) peak, and the identification of Q^3(1Al) sites, as reported in Table 3. The observation of Q^3(1Al) sites in these materials is an indication of crosslinking taking place in the C-A-S-H phase[48]. Although these pastes contain ettringite, which consumes some of the Al supplied by the slag, the content of hydrotalcite is notably lower than in the $Ba(OH)_2$-activated and NaOH-activated pastes (Figure 2), and so the availability of Al appears sufficient for this degree of substitution into the C-A-S-H. The fate of the Mg is, however, unclear at this stage. These results suggest that the structure of the C-A-S-H type gel forming in the composite binders is a result of a combined activation process involving both Na_2SO_4 and $Ba(OH)_2$, as the hydrate phase assemblages do not match what would be observed if the slag was solely activated by the NaOH produced in reaction (1). The C-A-S-H type binders forming in the composite specimens have a high degree of crosslinking associated with the high fractions of Q^2 and Q^3 species.

According to the quantification of Si sites presented in Table 3, it is observed from the remnant unreacted slag fraction that the lowest degree of reaction is achieved in the specimen activated solely with Na_2SO_4, and the highest degree of reaction when $Ba(OH)_2$ is used as the sole activator. These observations are in agreement with the thermogravimetry results, where the highest weight loss was identified in the $Ba(OH)_2$-activated specimens among all single-activator systems analysed. This demonstrates that $Ba(OH)_2$ can act as an effective activator for producing alkali-activated materials. Consequently, it is likely that the reaction of the composites assessed here is not exclusively governed by the formation of NaOH as a secondary product during the reaction of $Ba(OH)_2$ and Na_2SO_4 to form $BaSO_4$ (reaction 1), but rather that the original $Ba(OH)_2$ and Na_2SO_4 components are also having a significant impact. The higher reaction extent observed in M1.3 compared to M1.0 also indicates that the excess $Ba(OH)_2$ present in this mix leads to an increased extent of reaction.

Table 3. Quantification of Q^n environments identified in the ^{29}Si MAS NMR spectra of the specimens investigated.

Sample ID	*Unreacted slag*	*Site type in reaction products*[a]						
		Q^0	***$Q^1(I)$***	***$Q^1(II)$***	***$Q^2(1Al)$***	***Q^2***	***$Q^3(1Al)$***	***$Q^3(0Al)$***
		-74	***-78***	***-80***	***-82***	***-85***	***-89***	***-94***
M1.0	47	9	4	9	12	11	7	2
M1.3	45	9	5	9	11	13	6	2
Na_2SO_4	53	10	6	3	7	12	7	3
NaOH	49	10	5	11	12	10	3	-

$Ba(OH)_2$	39	9	5	9	13	16	7	2

[a] Estimated uncertainty in all site percentages is ± 2%, based on the influence of the signal/noise ratio of the spectra on the de-convolution procedures.

3.4 Solid-state ^{27}Al MAS NMR spectroscopy

Figure 7 shows the ^{27}Al MAS NMR spectra of the samples evaluated. The unreacted BFS shows a broad resonance between 40 and 80 ppm, centred around 60 ppm. This region is assigned to tetrahedral Al environments, but cannot be assigned to a well-defined single site type due to structural disorder in the slag. This broad peak is attributed to the glassy phases which comprise the majority of the BFS, consistent with the amorphous hump and low crystalline phase content identified by XRD in the unreacted BFS (Figure 1).

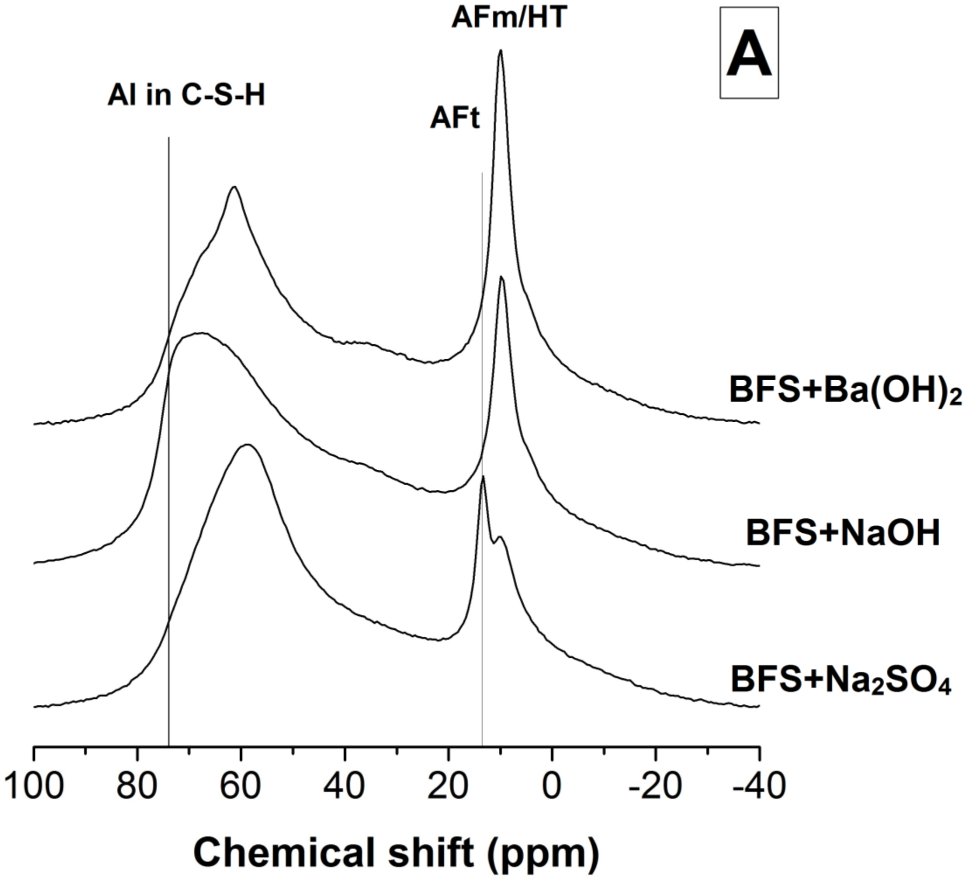

Postprint of a paper published in *Cement and Concrete Research*, 66(2014):64-74. Version of record is available at http://dx.doi.org/10.1016/j.cemconres.2014.07.006

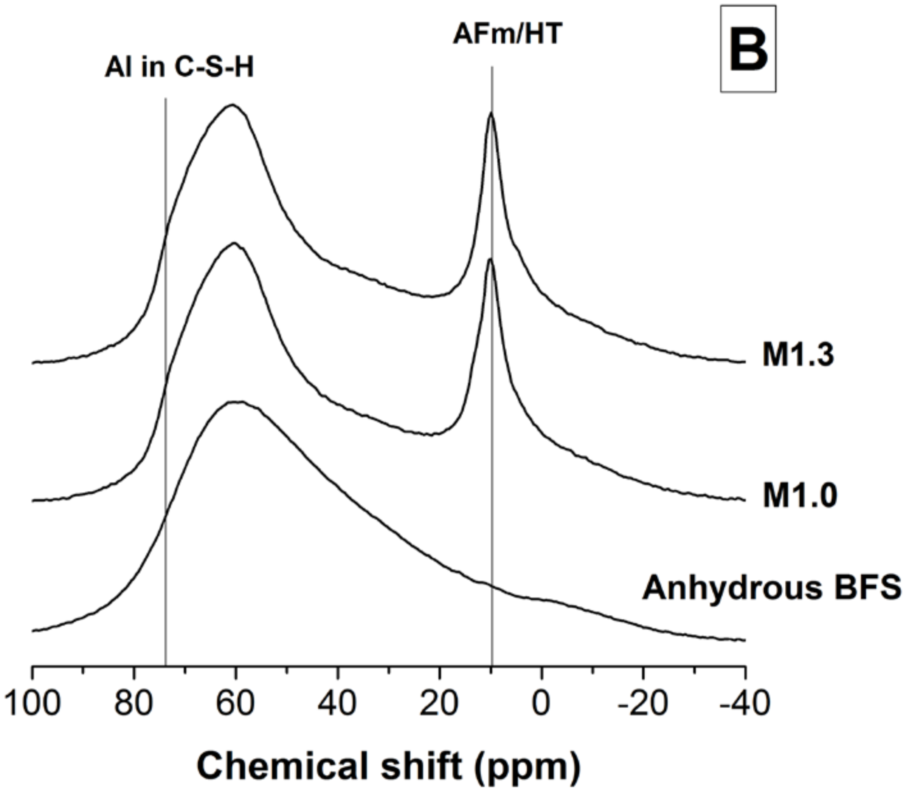

Figure 7. ^{27}Al MAS NMR spectra of (A) Na_2SO_4-activated BFS, NaOH-activated BFS and $Ba(OH)_2$-activated BFS pastes, and (B) unreacted slag, and $Ba(OH)_2$-Na_2SO_4 slag composites M1.0 and M1.3.

In the Na_2SO_4-activated BFS sample (Figure 7A), there are two distinguishable peaks in the region associated with octahedrally coordinated Al. The larger peak in this region, at around 13 ppm, is assigned to ettringite [49] as identified by XRD (Figure 1). The shoulder at 10 ppm is assigned to the hydrotalcite type phase [43] also observed by XRD in this sample, which may also contain minor contributions from AFm type phases as suggested by the DTG analysis, although these are not positively identifiable by XRD. In the NaOH-activated and $Ba(OH)_2$-activated pastes, a single peak at 10 ppm is observed in this region of the spectra, and attributed to the layered double hydroxide and AFm type phases, which have very similar ^{27}Al resonance positions.

The main effect of the activator is identified in the region between 40 ppm and 80 ppm in Figure 7, which is associated with the tetrahedrally coordinated Al. Upon activation a sharpening of the Al(IV) region is identified in all the samples compared with the unreacted BFS; as not all of the slag has reacted, part of the intensity of this band should be assigned to the remnant unreacted BFS. In C-A-S-H products, Al is tetrahedrally coordinated and usually identified at 74 ppm in ^{27}Al MAS NMR spectra [28, 47]. This resonance is observed in NaOH and Ba(OH)$_2$ activated pastes, consistent with the identification in the ^{29}Si MAS NMR results (Table 3) of high intensity peaks assigned to Q^2(1Al) sites.

In the Na$_2$SO$_4$-activated paste, an asymmetric Al(IV) band with a maximum at 60 ppm is instead observed. This resonance is assigned to highly crosslinked Al-rich sites in the C-A-S-H type gel, in agreement with the identification of Q^3(1Al) sites by ^{29}Si MAS NMR. In the Ba(OH)$_2$-activated sample a high intensity peak centred at 61 ppm is identified. Resonances at this specific chemical shift value are consistent with the formation of an poorly ordered AFm type phase (strätlingite) in Al-rich cementitious systems formed under high alkalinity conditions [50]; however, studies of Ba-bearing AFm and/or hydrogarnet phases are very limited, and ^{27}Al MAS NMR spectra of compounds with such chemistry are not available in the open literature to corroborate the assignment of this peak. Considering that Q^3 type sites are observed in the Ba(OH)$_2$ activated sample in the ^{29}Si MAS NMR spectra, and these sites can be also present in hydrogarnet type phases [51], it is suggested that the formation of a Ba-bearing AFm or hydrogarnet type phase might be occurring. Further investigation to validate this hypothesis is required.

In the Ba(OH)$_2$-Na$_2$SO$_4$-BFS composite samples (Figure 7B) a broad band around 10 ppm with less distinct features than those identified in the NaOH-activated or Ba(OH)$_2$-activated slags is observed, and again assigned to the contributions of hydrotalcite type-and ettringite phases, as identified through XRD (Figure 1). The lineshape of the Al(IV) region of the composite spectra does not show significant changes with the addition of different amounts of Ba(OH)$_2$, consistent with the observation that the C-A-S-H products forming in these systems have very similar structures, as identified via ^{29}Si MAS NMR (Figure 6).

3.5 Solid-state ^{23}Na MAS NMR

Figure 8 shows the ^{23}Na MAS NMR results for anhydrous Na$_2$SO$_4$, Na$_2$SO$_4$-activated slag and Ba(OH)$_2$-Na$_2$SO$_4$ slag composite cements. The spectrum collected for anhydrous Na$_2$SO$_4$ is used here as a reference to identify unreacted Na$_2$SO$_4$ in the samples. The line shape of the Na$_2$SO$_4$ spectrum is in good agreement with those reported in the literature [52]. It is clear from the spectra of the Na$_2$SO$_4$-activated slag and the composite M1.0 sample that there is some unreacted Na_2SO_4 present in both of these mixes, visible particularly from the sharp resonance at -21 ppm which is seen as a shoulder in the reaction product spectra. This indicates that in the absence of $Ba(OH)_2$, although some of the sulphate in the waste simulant is chemically bonded through the formation of ettringite, there is an excess of sulphate that is likely to be remaining in the pore solution, and then precipitating as Na_2SO_4 when the samples are dried for analysis. The inclusion of lower contents of $Ba(OH)_2$ (Figure 8 sample M1.0) reduces the remnant Na_2SO_4 in the sample, due to the formation of $BaSO_4$ as observed by other analytical techniques; however, there is not complete consumption of Na_2SO_4. This suggests the need for higher $Ba(OH)_2$ contents in the system in order to immobilise all of the sulphate bearing waste, as in composite M1.3, where ^{23}Na resonances assigned to remnant Na_2SO_4 are not identified.

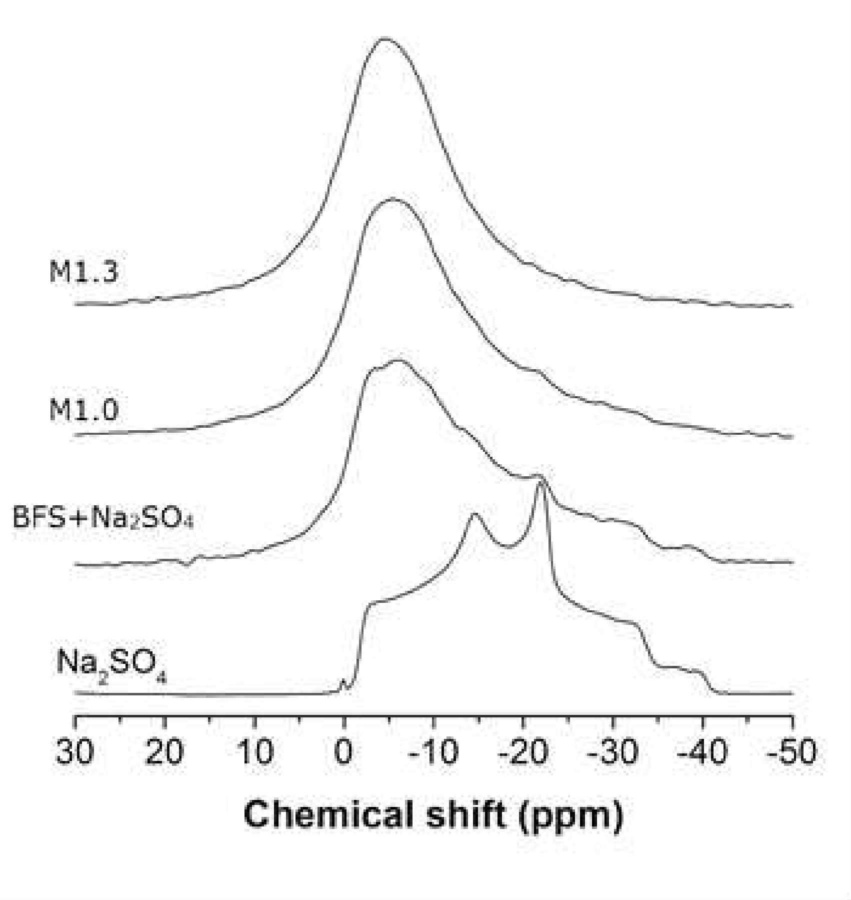

Figure 8. ^{23}Na MAS NMR spectra of Na_2SO_4, Na_2SO_4-activated BFS, and $Ba(OH)_2$-Na_2SO_4-BFS composite cements M1.0 and M1.3.

Alkalis play an important role in the properties and microstructure of the products formed during the alkali activation of BFS and aluminosilicate precursors [53]. It is believed that in alkali-activated slag binders, alkalis can be incorporated or physically adsorbed on the surface of the C-A-S-H products through a charge balance mechanism, and also exist free in the pore solution [54, 55]. However, it is likely that the mechanism of uptake of alkalis into the solid phases in alkali-activated materials is strongly dependent on the type of activator used, as this controls the Ca/(Si+Al) ratio of the C-A-S-H type gels, which can vary over the time of curing [20, 26, 56].

In the alkali-activated composites studied here, a ^{23}Na resonance at around -6 ppm is observed (Figure 8), consistent with the results reported by Bonk et al. [23] for the alkalis in C-A-S-H type gels in alkali-activated slag binders, analysed at a comparable magnetic field. Formation of C-(N)-A-S-H binding phases has been identified in alkali-activated slags via microscopy techniques [18, 57], and it has been proposed that the inclusion of alkalis in the C-A-S-H gel can occurs via a charge balancing mechanism where the charge deficit associated with the replacement of a bridging SiO_4 tetrahedron with an AlO_4 unit is balanced by an alkali ion adsorbed/bonded in the interlayer region of the C–S–H phase [58]. It is also clear from the ^{23}Na MAS NMR spectra that the peak at -6 ppm is narrowed in the composite sample M1.3, with a higher amount of $Ba(OH)_2$, indicating a more ordered gel structure.

3.6 Scanning electron microscopy

Figure 9 shows a backscattered electron (BSE) image of the BFS activated with Na_2SO_4, and elemental distribution in the region of the image. Regions enriched in Ca, Si, Al and Mg correspond to the unreacted slag, whose angular morphology is clear as light grey isolated regions. The binder matrix is mainly composed of Ca, Si and Al, consistent with the formation of a C-A-S-H product, as identified by NMR spectroscopy. An even distribution of Na throughout the binding phase is also observed, consistent with the inclusion of Na in the C-A-S-H type phase as discussed in the analysis of the ^{23}Na MAS NMR results. The regions poor in Si but rich in S (white circles in Figure 9) are identified as ettringite.

Postprint of a paper published in *Cement and Concrete Research*, 66(2014):64-74. Version of record is available at http://dx.doi.org/10.1016/j.cemconres.2014.07.006

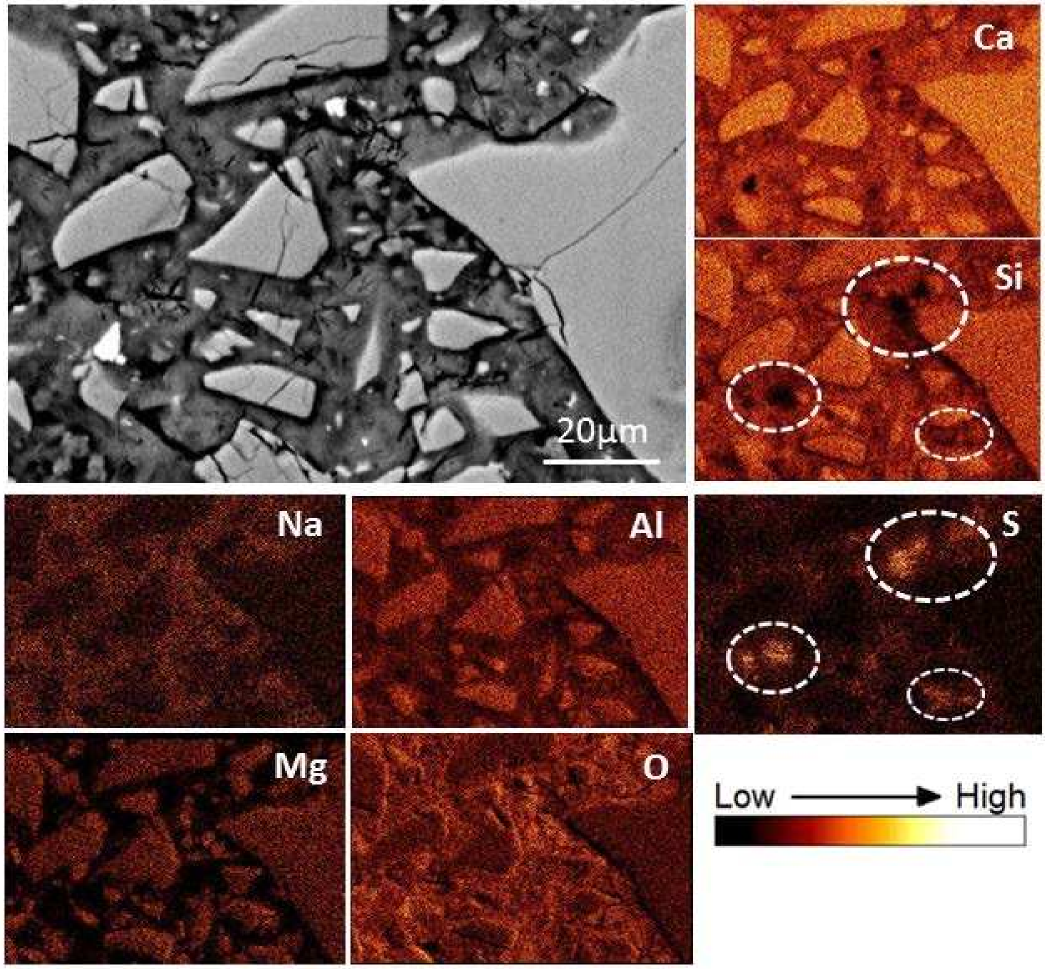

Figure 9. Backscattered electron image and elemental maps of Na_2SO_4-activated BFS. The elemental maps show the same region as the backscattered electron image.

Figure 10 shows a BSE image of the BFS sample activated by $Ba(OH)_2$, and the elemental maps corresponding to this image. This binder shows a highly heterogeneous matrix, with cavities due to the pull-out of unreacted slag particles during sample polishing, as the unreacted slag grains are surrounded by a low-density reaction rim which appears to give little binding to the bulk gel. This is supported by the fact that the cavities (black areas) observed in the BSE have an angular shape consistent with the shape of unreacted slag particles, which would not be the case if those cavities were pores. It is clear from Ba elemental mapping that Ba is incorporated relatively homogenously throughout the binding matrix, suggesting that the inclusion of some Ba in the C-A-S-H might be occurring in this system. Formation of a C-(Ba)-A-S-H gel has not been observed before, but these results indicate that excess Ba in Ca-rich cementitious systems is not only able to influence sulphate and carbonate rich phases, as has been observed with the inclusion of $BaCO_3$ [33, 36], but also possibly participate in the C-A-S-H type phase if the concentrations of sulphate and carbonate are low.

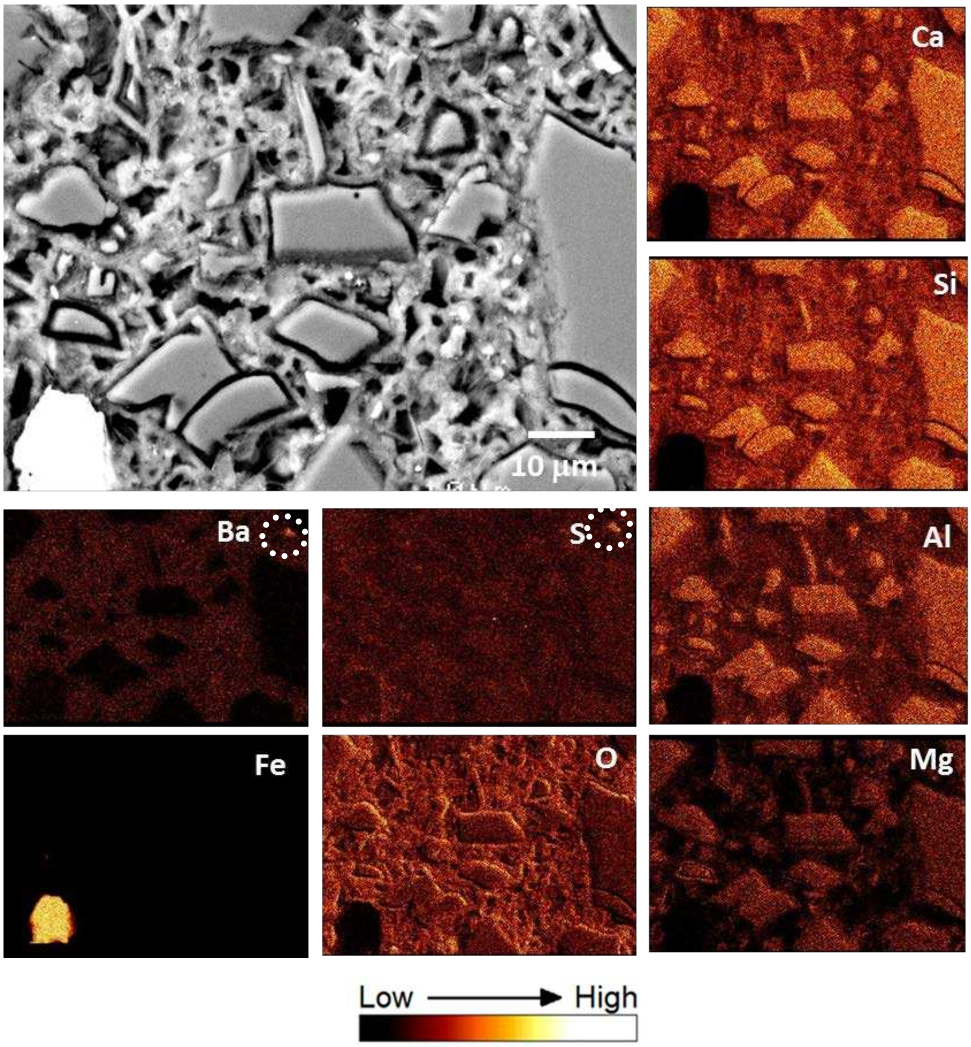

Figure 10. Backscattered electron image and elemental maps of $Ba(OH)_2$-activated slag. The elemental maps show the same region as the backscattered electron image. Dashed circles in Ba and S maps highlight a $BaSO_4$ particle forming in this system

In Figure 10, there is also a small region (dashed circles in Ba and S maps) with an increased concentration of Ba and S, indicating the formation of $BaSO_4$, with the sulphate presumably made available through oxidation of the sulphide supplied by the slag. Sulphur appears to be homogenously distributed in the unreacted slag particles and also the matrix, but it is particularly concentrated around the edge of what appears to be a Fe particle observed in the bottom left of the micrograph (the bright white particle in the BSE image). This Fe-S rich region is likely to correspond to an iron sulphide FeS_x ($1 \leq x \leq 2$), consistent with the highly reducing environment in slag-rich cements [59].

Figure 11 shows a BSE image of the M1.0 sample, together with the elemental distributions of sulphur and barium in the corresponding region. Angular BFS particles are dispersed throughout the binding C-A-S-H phase. The formation of $BaSO_4$ is observed as both small and larger white particles in the BSE image, confirmed by the corresponding elemental maps. Some of the $BaSO_4$ particles appear to form particularly in the area surrounding the slag particles. This indicates that Ba will react not just with the sulphur supplied by the sulphate bearing solution, but also with the sulphur present in the slag, as noted above.

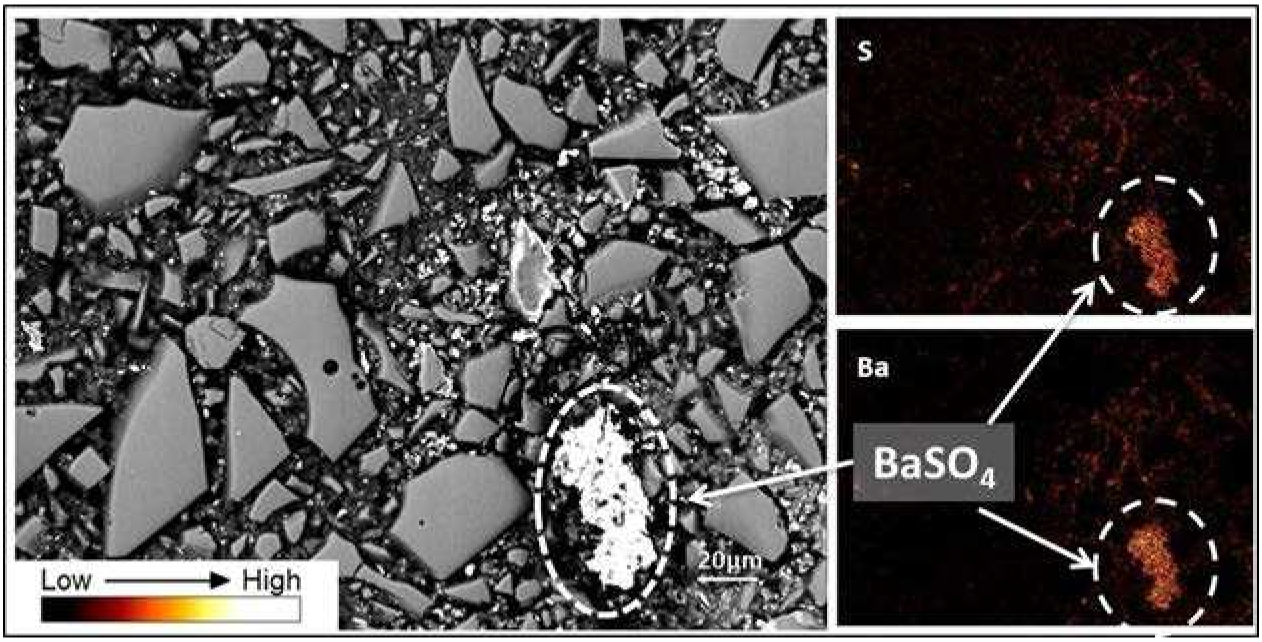

Figure 11. Backscattered electron image and elemental maps of sample M1.0. Ba and S elemental maps confirm the formation of $BaSO_4$

Figure 12 shows another region of the composite sample M1.0, where a homogeneous C-A-S-H binding matrix (dark grey area), with embedded unreacted slag particles (light grey) and $BaSO_4$ particles (white particles), is observed. The inset shows a higher magnification image of a region with reduced content of $BaSO_4$ particles, where it is possible to identify the formation of phases with microstructures comparable to the lamellar morphology observed for monosulphoaluminate/ettringite compounds [60], consistent with the mineralogy identified by other analytical techniques here. The EDX spectrum of this region shows the incorporation of Ba in these sulphoaluminate phases, supporting the formation of a Ba-substituted ettringite as previously suggested based on XRD data.

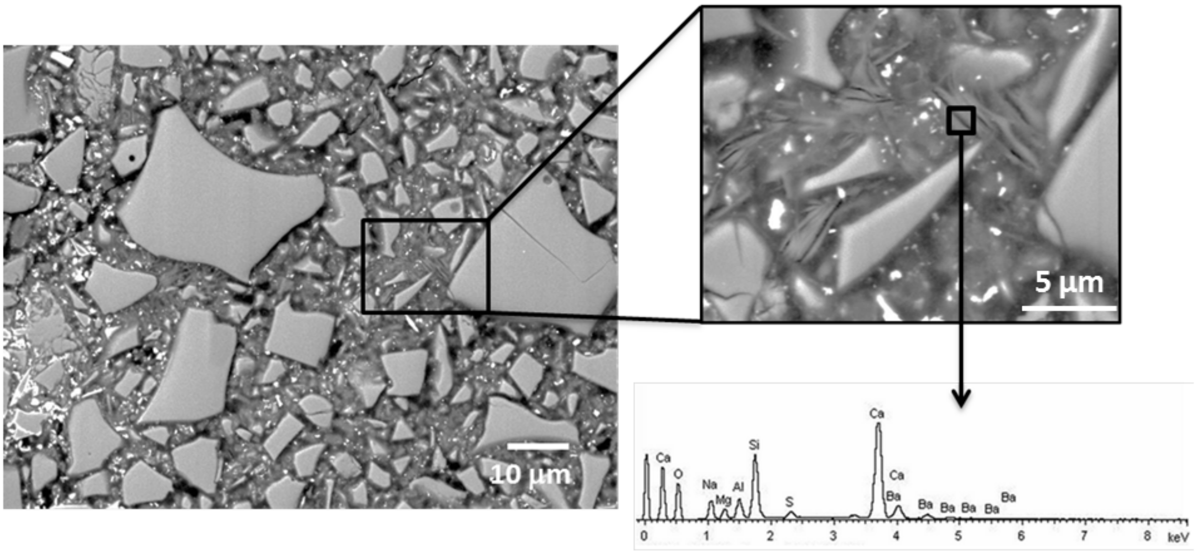

Figure 12. Backscattered electron image of sample M1.0, with a higher-magnification view of the sulphoaluminate product formed within the gel, and an EDX spectrum of the region indicated.

4. Conclusions

Solid composite cement binders in the system $Ba(OH)_2$-Na_2SO_4-slag can be produced via a one-step method for immobilisation of sulphate bearing aqueous nuclear waste, where the precipitation of $BaSO_4$ generates NaOH in situ to act as an activator for the slag, in addition to the individual effects of the $Ba(OH)_2$ and Na_2SO_4. X-ray diffraction results confirm the successful binding of sulphate in very insoluble crystalline phases such as $BaSO_4$ in the composite samples, offering the potential for good binder stability in the long term. The microstructure of the composites is dominated by the strength giving phase C-A-S-H, along with layered double hydroxides (hydrotalcite and AFm type) and Ba-substituted ettringite forming as secondary reaction products. Comparing the reaction products formed in the composite wasteforms with those identified when activating BFS with either $Ba(OH)_2$, Na_2SO_4 or NaOH as a sole activator, it is seen that both Na_2SO_4 and $Ba(OH)_2$ are acting as alkaline activators in the composite system. An increased content of $Ba(OH)_2$ in the composite binders seems to favour a higher extent of reaction of the slag, and a 30% excess of $Ba(OH)_2$ over Na_2SO_4 is seen to be sufficient to prevent the presence of free Na_2SO_4 in the pore network of the binder. The inclusion of Ba also influences the chemistry of the main reaction products in these composites; Ba^{2+} is able to substitute into ettringite, which reduces the formation of hydrotalcite in the composite cements compared to those activated by a sole activator. There also appears to be some scope for substitution of Ba^{2+} for Ca^{2+} in C-A-S-H gel, particularly when no sulphate is added.

Acknowledgements

This study has been sponsored by EPSRC through the ‘Nuclear FiRST’ Doctoral Training Centre at The University of Sheffield and The University of Manchester. The NMR spectra were collected using the EPSRC UK National Solid-state NMR Service at Durham University. The authors would like to thank Dr. Claire Utton for valuable comments and discussions regarding this work, and Dr Clint Sharrad for his input into the PhD project of NM.

References

[1] P.A. Bingham, R.J. Hand, Sulphate incorporation and glass formation in phosphate systems for nuclear and toxic waste immobilization, Mater. Res. Bull., 43 (2008) 1679-1693.
[2] R.S. Gollop, H.F.W. Taylor, Microstructural and microanalytical studies of sulfate attack. IV. Reactions of a slag cement paste with sodium and magnesium sulfate solutions, Cem. Concr. Res., 26 (1996) 1013-1028.
[3] H.F.W. Taylor, C. Famy, K.L. Scrivener, Delayed ettringite formation, Cem. Concr. Res., 31 (2001) 683-693.
[4] F.P. Glasser, Progress in the immobilization of radioactive wastes in cement, Cem. Concr. Res., 22 (1992) 201-216.
[5] T. Asano, T. Kawasaki, N. Higuchi, Y. Horikawa, Feasibility study of solidification for low-level liquid waste generated by sulfuric acid elution treatment of spent ion exchange resin, J Power Energy Syst, 2 (2008) 206-214.
[6] N. Mobasher, H. Kinoshita, S.A. Bernal, C.A. Sharrad, $Ba(OH)_2$ – blast furnace slag composite binders for the encapsulation of sulphate bearing nuclear waste, Advances in Applied Ceramics, (2014), in press, DOI 10.1179/1743676114Y.0000000148.
[7] D.R. Lide, CRC Handbook of Chemistry and Physics, 86th ed., Taylor and Francis, USA, 2005.
[8] Y. Esen, B. Yilmazer, An investigation of X-ray and radio isotope energy absorption of heavyweight concretes containing barite, Bull. Mater. Sci., 34 (2011) 169-175.
[9] IAEA, Handling and Processing of Radioactive Waste for Nuclear Applications, Technical Report, Vienna, 2001.
[10] S.A. Bernal, J.L. Provis, A. Fernández-Jiménez, P.V. Krivenko, E. Kavalerova, M. Palacios, C. Shi, Binder chemistry – High-calcium alkali-activated materials. In: Alkali-Activated Materials:

State-of-the-Art Report, RILEM TC 224-AAM, editors J.L. Provis, J.S.J. van Deventer, RILEM/Springer, Dordrecht, 2014, 59-91.

[11] C. Shi, A. Fernández-Jiménez, Stabilization/solidification of hazardous and radioactive wastes with alkali-activated cements, J. Hazard. Mater., B137 (2006) 1656-1663.

[12] S.-D. Wang, X.-C. Pu, K.L. Scrivener, P.L. Pratt, Alkali-activated slag cement and concrete: a review of properties and problems, Adv. Cem. Res., 7 (1995) 93-102.

[13] I.G. Richardson, The nature of C-S-H in hardened cements, Cem. Concr. Res., 29 (1999) 1131-1147.

[14] A. Fernández-Jiménez, F. Puertas, I. Sobrados, J. Sanz, Structure of calcium silicate hydrates formed in alkaline-activated slag: Influence of the type of alkaline activator, J. Am. Ceram. Soc., 86 (2003) 1389-1394.

[15] I.G. Richardson, G.W. Groves, Microstructure and microanalysis of hardened cement pastes involving ground granulated blast-furnace slag, J. Mater. Sci., 27 (1992) 6204-6212.

[16] O. Burciaga-Díaz, J.I. Escalante-García, Structure, mechanisms of reaction, and strength of an alkali-activated blast-furnace slag, J. Am. Ceram. Soc., 96 (2013) 3939-3948.

[17] M. Ben Haha, B. Lothenbach, G. Le Saout, F. Winnefeld, Influence of slag chemistry on the hydration of alkali-activated blast-furnace slag -- Part I: Effect of MgO, Cem. Concr. Res., 41 (2011) 955-963.

[18] M. Ben Haha, B. Lothenbach, G. Le Saout, F. Winnefeld, Influence of slag chemistry on the hydration of alkali-activated blast-furnace slag — Part II: Effect of Al_2O_3, Cem. Concr. Res., 42 (2012) 74-83.

[19] S.A. Bernal, R. San Nicolas, R.J. Myers, R. Mejía de Gutiérrez, F. Puertas, J.S.J. van Deventer, J.L. Provis, MgO content of slag controls phase evolution and structural changes induced by accelerated carbonation in alkali-activated binders, Cem. Concr. Res., 57 (2014) 33-43.

[20] M. Ben Haha, G. Le Saout, F. Winnefeld, B. Lothenbach, Influence of activator type on hydration kinetics, hydrate assemblage and microstructural development of alkali activated blast-furnace slags, Cem. Concr. Res., 41 (2011) 301-310.

[21] S.D. Wang, K.L. Scrivener, Hydration products of alkali-activated slag cement, Cem. Concr. Res., 25 (1995) 561-571.

[22] P.J. Schilling, L.G. Butler, A. Roy, H.C. Eaton, ^{29}Si and ^{27}Al MAS-NMR of NaOH-activated blast-furnace slag, J. Am. Ceram. Soc., 77 (1994) 2363-2368.

[23] F. Bonk, J. Schneider, M.A. Cincotto, H. Panepucci, Characterization by multinuclear high-resolution NMR of hydration products in activated blast-furnace slag pastes, J. Am. Ceram. Soc., 86 (2003) 1712-1719.

[24] A. Gruskovnjak, B. Lothenbach, F. Winnefeld, R. Figi, S.C. Ko, M. Adler, U. Mäder, Hydration mechanisms of super sulphated slag cement, Cem. Concr. Res., 38 (2008) 983-992.

[25] Y. Bai, N.C. Collier, N.B. Milestone, C.H. Yang, The potential for using slags activated with near neutral salts as immobilisation matrices for nuclear wastes containing reactive metals, J. Nucl. Mater., 413 (2011) 183-192.

[26] J. Escalante-Garcia, A.F. Fuentes, A. Gorokhovsky, P.E. Fraire-Luna, G. Mendoza-Suarez, Hydration products and reactivity of blast-furnace slag activated by various alkalis., J. Am. Ceram. Soc., 86 (2003) 2148-2153.

[27] S.-D. Wang, K.L. Scrivener, ^{29}Si and ^{27}Al NMR study of alkali-activated slag, Cem. Concr. Res., 33 (2003) 769-774.

[28] I.G. Richardson, A.R. Brough, R. Brydson, G.W. Groves, C.M. Dobson, Location of aluminum in substituted calcium silicate hydrate (C-S-H) gels as determined by ^{29}Si and ^{27}Al NMR and EELS, J. Am. Ceram. Soc., 76 (1993) 2285-2288.

[29] F.P. Glasser, Chemistry of solidified waste forms, in: R.D. Spence (Ed.) Chemistry and Microstructure of Solidified Waste Forms, Boca Raton:Lewis Publishers, US, 1993.

[30] F. Glasser, A. Kindness, S. Stronach, Stability and solubility relationships in AFm phases: Part I. Chloride, sulfate and hydroxide, Cem. Concr. Res., 29 (1999) 861-866.

[31] M.L.D. Gougar, B.E. Scheetz, D.M. Roy, Ettringite and C-S-H Portland cement phases for waste ion immobilization: A review, Waste Manag., 16 (1996) 295-303.

[32] C. Jun, C. Xin, L. Lingchao, H. Shifeng, Y. Zhengmao, High water content material based on ba-bearing sulphoaluminate cement, J. Wuhan Univ. Technol.-Mater. Sci. Ed., 20 (2005) 88-90.

[33] C.A. Utton, E. Gallucci, J. Hill, N.B. Milestone, Interaction between $BaCO_3$ and OPC/BFS composite cements at 20°C and 60°C, Cem. Concr. Res., 41 (2011) 236-243.

[34] D. Dermatas, X. Meng, Utilization of fly ash for stabilization/solidification of heavy metal contaminated soils, Eng. Geol., 70 (2003) 377-394.

[35] E. Ciliberto, S. Ioppolo, F. Manuella, Ettringite and thaumasite: A chemical route for their removal from cementious artefacts, J. Cult. Herit., 9 (2008) 30-37.

[36] P.M. Carmona-Quiroga, M.T. Blanco-Varela, Ettringite decomposition in the presence of barium carbonate, Cem. Concr. Res., 52 (2013) 140-148.

[37] C. Hall, P. Barnes, A.D. Billimore, A.C. Jupe, X. Turrillas, Thermal decomposition of ettringite $Ca_6[Al(OH)_6]_2(SO_4)_3.26H_2O$, J. Chem. Soc. Faraday Trans., 92 (1996) 2125-2129.

[38] L. Alarcon-Ruíz, G. Platret, E. Massieu, A. Ehrlacher, The use of thermal analysis in assessing the effect of temperature on a cement paste, Cem. Concr. Res., 35 (2005) 609-613.

[39] M. Maciejewski, H.-R. Oswald, A. Reller, Thermal transformations of vaterite and calcite, Thermochim. Acta, 234 (1994) 315-328.

[40] E. Kanezaki, Thermal behavior of the hydrotalcite-like layered structure of Mg and Al-layered double hydroxides with interlayer carbonate by means of in situ powder HTXRD and DTA/TG, Solid State Ionics, 106 (1998) 279-284.

[41] V.S. Ramachandran, C.-M. Zhang, Thermal analysis of the $3CaO\cdot Al_2O_3$-$CaSO_4\cdot 2H_2O$-$CaCO_3$-H_2O system, Thermochim. Acta, 106 (1986) 273-282.

[42] K. Rozov, U. Berner, C. Taviot-Gueho, F. Leroux, G. Renaudin, D. Kulik, L.W. Diamond, Synthesis and characterization of the LDH hydrotalcite–pyroaurite solid-solution series, Cem. Concr. Res., 40 (2010) 1248-1254.

[43] S.A. Bernal, J.L. Provis, B. Walkley, R. San Nicolas, J.D. Gehman, D.G. Brice, A.R. Kilcullen, P. Duxson, J.S.J. van Deventer, Gel nanostructure in alkali-activated binders based on slag and fly ash, and effects of accelerated carbonation, Cem. Concr. Res., 53 (2013) 127-144.

[44] G. Engelhardt, D. Michel, High-Resolution Solid-State NMR of Silicates and Zeolites, John Wiley & Sons, Chichester, 1987.

[45] J.R. Barnes, A.D.H. Clague, N.J. Clayden, C.M. Dobson, C.J. Hayes, G.W. Groves, S.A. Rodger, Hydration of Portland cement followed ^{29}Si solid-state NMR spectroscopy, J. Mater. Sci. Lett., 4 (1985) 1293-1295.

[46] G. Le Saoût, M. Ben Haha, F. Winnefeld, B. Lothenbach, Hydration degree of alkali-activated slags: A ^{29}Si NMR study, J. Am. Ceram. Soc., 94 (2011) 4541-4547.

[47] M.D. Andersen, H.J. Jakobsen, J. Skibsted, Incorporation of aluminum in the calcium silicate hydrate (C−S−H) of hydrated Portland cements: A high-field ^{27}Al and ^{29}Si MAS NMR investigation, Inorg. Chem., 42 (2003) 2280-2287.

[48] R.J. Myers, S.A. Bernal, R. San Nicolas, J.L. Provis, Generalized structural description of calcium-sodium aluminosilicate hydrate gels: the cross-linked substituted tobermorite model, Langmuir, 17 (2013) 5294-5306.

[49] M.D. Andersen, H.J. Jakobsen, J. Skibsted, A new aluminium-hydrate species in hydrated Portland cements characterized by ^{27}Al and ^{29}Si MAS NMR spectroscopy, Cem. Concr. Res., 36 (2006) 3-17.

[50] S. Kwan, J. LaRosa, M.W. Grutzeck, ^{29}Si and ^{27}Al MASNMR study of strätlingite, J. Am. Ceram. Soc., 78 (1995) 1921-1926.

[51] J.M. Rivas Mercury, P. Pena, A.H. De Aza, X. Turrillas, I. Sobrados, J. Sanz, Solid-state ^{27}Al and ^{29}Si NMR investigations on Si-substituted hydrogarnets, Acta Mater., 55 (2007) 1183-1191.

[52] H. Koller, G. Engelhardt, A.P.M. Kentgens, J. Sauer, ^{23}Na NMR spectroscopy of solids: Interpretation of quadrupole interaction parameters and chemical shifts, J. Phys. Chem., 98 (1994) 1544-1551.

[53] C. Shi, P.V. Krivenko, D.M. Roy, Alkali-Activated Cements and Concretes, Taylor & Francis, Abingdon, UK, 2006.

[54] C. Shi, On the state and role of alkalis during the activation of alkali-activated slag cement, in: Proceedings of the 11th International Congress on the Chemistry of Cement, Durban, South Africa, 2003.

[55] T.T.H. Bach, E. Chabas, I. Pochard, C. Cau Dit Coumes, J. Haas, F. Frizon, A. Nonat, Retention of alkali ions by hydrated low-pH cements: Mechanism and Na^+/K^+ selectivity, Cem. Concr. Res., 51 (2013) 14-21.
[56] F. Puertas, A. Fernández-Jiménez, M.T. Blanco-Varela, Pore solution in alkali-activated slag cement pastes. Relation to the composition and structure of calcium silicate hydrate, Cem. Concr. Res., 34 (2004) 139-148.
[57] S.A. Bernal, J.L. Provis, V. Rose, R. Mejía de Gutiérrez, High-resolution X-ray diffraction and fluorescence microscopy characterization of alkali-activated slag-metakaolin binders, J. Am. Ceram. Soc., 96 (2013) 1951-1957.
[58] J. Skibsted, M.D. Andersen, The effect of alkali ions on the incorporation of aluminum in the calcium silicate hydrate (C–S–H) phase resulting from Portland cement hydration studied by ^{29}Si MAS NMR, J. Am. Ceram. Soc., 96 (2012) 651-656.
[59] M. Atkins, F.P. Glasser, Application of Portland cement-based materials to radioactive waste immobilization, Waste Manag., 12 (1992) 105-131.
[60] K.L. Scrivener, Backscattered electron imaging of cementitious microstructures: understanding and quantification, Cem. Concr. Compos., 26 (2004) 935-945.